Springer

KSME

Journal of Mechanical Science and Technology 24 (8) (2010) 1573~1581
www.springerlink.com/content/1738-494x
DOI 10.1007/s12206-010-0506-1

Influence of rub groove on rotordynamics associated with leakage air flow through a labyrinth seal †

Wei Zhe Wang [1], Ying Zheng Liu[1*], Guang Meng[2] and Pu Ning Jiang[3]

[1]*Key Lab of Education Ministry for Power Machinery and Engineering, Shanghai Jiao Tong University,800 Dongchuan Road, Shanghai 200240, China*
[2]*State Key Lab of Mechanical System and Vibration, Shanghai Jiao Tong University,800 Dongchuan Road, Shanghai 200240, China*
[3]*Department of R&D, Shanghai Turbine Company,333 Jiang Chuan Road, Shanghai 200240, China*

(Manuscript Received June 17, 2009; Revised January 11, 2010; Accepted April 22, 2010)

Abstract

An extensive investigation of influence of rub grooves on dynamics and stability of the rotor, which is subjected to aerodynamic forcing associated with the leakage flow through 44 straight-through seals, was performed by using numerical calculations based on the single control-volume method and the perturbation analysis. Three cases of different groove configurations were chosen for the comparative study, e.g., the seal without rub groove (case1), the seal with upstream shifting of the seal tooth in respect to the rub groove (case2) and the seal with location of the seal tooth in the middle station of the rub groove (case3). The orifice contract coefficient adopted in reduction of rotordynamic coefficients was provided by using Computational Fluid Dynamics (CFD). Influence of rub grooves on the leakage flow was obtained in terms of the close-up view of the flow pattern near the seal tooth, leakage flow rate, distributions of the mean pressure and circumferential velocity in cavities. In comparison to case 1, the leakage flow in case 3 is considerably intensified, while which in case 2 is slightly increased. Dynamics and instability of the rotor in all cases was discussed in terms of the rotordynamic coefficients and the logarithmic decrement, respectively. The results disclosed that the aerodynamic forcing in case 2 intensified the destabilization of the rotor system.

Keywords: Straight-through seal; Rub groove; Rotordynamic; Perturbation analysis

1. Introduction

Labyrinth seals closely spaced between the rotor and stator in turbomachinery are widely designed to keep a fine clearance at the order of 10^{-1} mm in a view to suppress the leakage. However, rubbing of tooth tips against the stator often occurs when the engine undergoes the transient operation like starting up and shutting down, creating rub grooves in the stator [1]. The presence of rub grooves would deteriorate the sealing performance or even induce the seal failure. Previous studies [2-4] have shown that leakage flow through labyrinth seals without rub grooves would give a significant influence on the rotor dynamics. Accordingly, an insight understanding of influence of rub grooves on dynamics of the rotor subjected to aerodynamic forcing of the leakage flow is of essential significance.

Various numerical and experimental efforts have been attempted to delineate the impairment of rub grooves to the sealing performance. Zimmermann et al. [5] numerically simulated leakage flow through the straight-through and stepped seals with fixed-size rub grooves, showing that the air leakage is increased substantially due to the presence of rub grooves. Subsequently, the slight influence of fixed-size rub grooves on leakage flow through the honeycomb seal with increasing the rotor speed and swirl velocity was presented by Yu and Childs [6]. The numerical study of leakage flow through stepped labyrinth seal with rub grooves of different size showed the peaked 94% increase of the leakage flow [7]. Xu et al. [8] numerically predicted the significant influence of rub groove shape on the leakage air flow rate and the flow pattern of the stepped seal. Visualizations of leakage flow through the labyrinth seal by Denecke et al. [9] demonstrated that the flow pattern is substantially changed when the labyrinth teeth enters into the rub groove. Rhode and Adams [10] numerically quantified variation of leakage air flow through the straight-through seal with the axial shifting of the labyrinth tooth in respect to rub grooves; this situation is resulted from different thermal expansion rates of the rotor and stator in the transient operation of the engines [11]. Recently, Childs et al. [12] and Graviss [13] claimed that variation of leakage flow through the liquid laminar-flow annular seal due to rub grooves would have significant influence on the rotordynamic

† This paper was recommended for publication in revised form by Associate Editor Eung-Soo Shin

* Corresponding author. Tel.: +86 21 3420 6869, Fax: +86 21 3420 6719
E-mail address: yzliu@sjtu.edu.cn

coefficients. However, a literature survey reveals that no study was made of influence of rub grooves on dynamics and stability of the rotor subjected to leakage air flow through the labyrinth seal.

The major objective of the present study was directed toward numerical prediction of influence of rub grooves on dynamics and stability of the rotating rotor subjected to aerodynamic forcing of leakage flow through the labyrinth seal. The straight-through seal as shown in Fig.1 (a) was chosen for the comparative study; two cases as shown in Fig.1 (b,c) were evaluated, which are different in the axial shift of the labyrinth tooth in respect to the rub grooves. The mathematical model based on the bulk-flow theory [14] and perturbation analysis [15] was employed in numerical calculations. In addition, the discharge coefficients of leakage through the tooth clearance were determined by using computational fluid dynamics (CFD). A comprehensive comparative analysis was given in terms of flow pattern, leakage rate, rotordynamic coefficients, pressure and circumferential velocity in cavities and the logarithmic decrement. The results demonstrated that the aerodynamic forcing associated with the leakage air flow in case 2 reduced the destabilization speed of the rotating rotor.

2. Mathematical model

In the following part, numerical prediction of the interaction between the aerodynamic forcing induced by the leakage flow and the whirling motion of the rotor was performed by using the single control-volume method [16] and perturbation analysis [14]. Details regarding the mathematical procedures can be found in Dursun [15].

2.1 Calculation of leakage air flow

The steady and axisymmetric state of the leakage flow through the rotor-seal system is established when the rotor concentrically rotates at a constant speed. The fluid flow is governed by the continuity equation, meaning that the mass flow rate m_i through the orifice between the seal tooth and the rotor is constant as i varies from 1 to N,

$$m_1 = m_2 = \cdots = m_i = \cdots = m_N = m_0 = C_0 C_1 A_n \sqrt{\frac{P_{0i-1} - P_{0i}}{RT}} \quad (1)$$

where m_0 is the steady-state leakage mass flow rate. The leakage air flow is taken to be uniformly distributed and expanded isothermally from cavity (i-1) to cavity (i). The above equation was employed to calculate the steady pressure distribution P_{0i} in cavities and the leakage flow rate m_0. The kinetic energy carry-over coefficient C_1 is referred to Dursun [15].The second part consisting of the paper body must be edited in double column format. Figures and tables should be located at top or bottom of either column.

The orifice contraction coefficient C_0 adopted in Eq. (1)

Table 1. Dimension of the straight-through seal (mm).

L_1	10	C_r	0.5
L_2	1.5	R_s	50
W	0.3	bi	0.6
B	2.5	h	0.3

Table 2. Operating conditions of the straight-through seal.

Inlet pressure (bar)	2,3,4,5,6,7
Outlet pressure (bar)	1
Inlet and outlet temperature (^{0}C):	20
Rotating speed: ω (rpm)	1000,2000,3000,4000,5000,6000
Inlet circumferential velocity: V_{in} (m/s)	0
Tooth number: N	44
Rotor radius: R_s (mm)	50

Table 3. Comparison of leakage flow determined by CFD and single control-volume method.

P_1 (kpa)	P_2 (kpa)	Case 1 (kg/m^2-s)	
		FLUENT	*Single control volume* (C_0=0.769)
102	101	37.79811	37.57908
104	101	65.6487	65.40062
106	101	84.44028	84.84037
108	101	100.3571	100.8518
P_1 (kpa)	P_2 (kpa)	Case 2 (kg/m^2-s)	
		FLUENT	*Single control volume* (C_0=0.631)
102	101	37.24306	37.25810
104	101	65.15537	64.83465
106	101	84.39532	84.09629
108	101	99.17635	99.98615
P_1 (kpa)	P_2 (kpa)	Case 3 (kg/m^2-s)	
		FLUENT	*Single control volume* (C_0=0.7764)
102	101	31.04009	30.36816
104	101	53.15086	52.86782
106	101	68.08709	68.58948
108	101	79.91087	81.55461

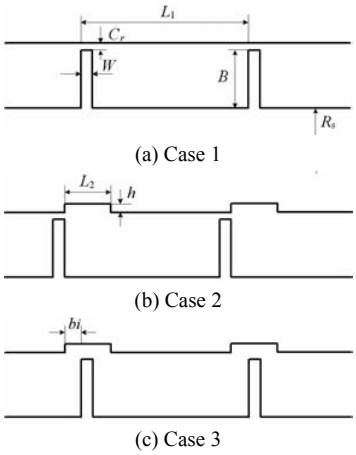

(a) Case 1

(b) Case 2

(c) Case 3

Fig. 1. Schematic diagram of the straight-through seals with and without rub grooves: (a) case 1, (b) case 2, (c) case 3.

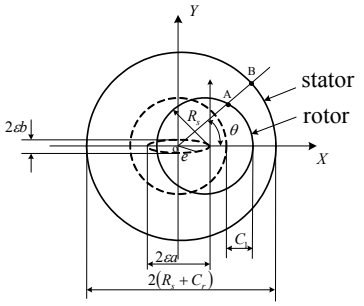

Fig. 2. Illustration of the elliptical orbit of the rotor.

accounts for the contraction of a jet emanating from a high pressure chamber through a planar orifice. The calculation of C_0 is related to the seal configuration and pressure ratio [17]. As the configuration of the labyrinth seal is fixed, C_0 is only influenced by the pressure ratio. In order to accurately obtain C_0 with varying the pressure ratio for the seal configurations shown in Fig. 1, the commercial package FLUENT 6.1 of computational fluid dynamics (CFD) was used to model the leakage flow through a single tooth clearance with high- and low-pressure chambers at its upstream and downstream sides, respectively. Accordingly, the coefficient C_0 was determined to 0.769, 0.631 and 0.7764 for the seal configurations of case 1, 2 and 3, respectively. The comparison of the leakage flow calculated by using CFD and Eq. (1) using the pre-defined coefficient C_0 was made at various conditions of pressure difference; as shown in Table.3, the favorable agreement of the leakage flow determined by using these two methods shows the reliability of the coefficient C_0 for each case, which will be hereafter employed in reduction of the first-order continuity and circumferential momentum equations.

When the critical condition appears at the last seal clearance, prediction of leakage flow is determined by,

$$m_0 = C_0 \mu P_{0N-1} \frac{A_n}{\sqrt{\gamma RT}} \left(\frac{2}{\gamma+1}\right)^{\left(\frac{\gamma}{\gamma-1}\right)} \tag{2}$$

2.2 First-order continuity and circumferential momentum equations

In practice, the inherent whirling motion of the rotor as shown in Fig. 2 implies that the leakage variables are actually unsteady and non-axisymmetric. Deviation of the flow variables like pressure, circumferential velocity and shear stress from the steady and axisymmetric state is dealt with by using perturbation analysis. As an example, the dependence of the circumferential velocity on the time t and the azimuthal position θ in each cavity is obtained by solving the partial differential continuity and circumferential momentum equations,

$$\begin{aligned} &\frac{\partial}{\partial t}(\rho_i A) + \frac{\rho_i V_i}{R_s}\frac{\partial A}{\partial \theta} + \frac{\rho_i A}{R_s}\frac{\partial V_i}{\partial \theta} + \frac{V_i A}{R_s}\frac{\partial \rho_i}{\partial \theta}, \\ &+\dot{q}_{i+1} - \dot{q}_i = 0 \end{aligned} \tag{3}$$

$$\begin{aligned} &\rho_i A\frac{\partial V_i}{\partial t} + \frac{\rho_i V_i A}{R_s}\frac{\partial V_i}{\partial \theta} + (V_i - V_{i-1})\dot{q}_i = \\ &-\frac{A}{R_s}\frac{\partial P_i}{\partial \theta} + (\tau_{ri}a_r - \tau_{si}a_s)L_1 \end{aligned}, \tag{4}$$

where

$$\begin{cases} A = L_1(B+H), & \text{for case1} \\ A = L_1(B+H) + L_2 \times h, & \text{for case2, case3} \end{cases}.$$

The parameters A and H vary in respect to (t,θ). The dimensionless shear stress lengths in Eq. (4) are defined by,

$$\begin{cases} a_r = \dfrac{2B+L_1}{L_1}, a_s = 1 & \text{for case1} \\ a_r = \dfrac{2B+L_1}{L_1}, a_s = \dfrac{2h+L_1}{L_1} & \text{for case2, case3} \end{cases} \tag{5}$$

Using Blasius formula, we define the shear stress at the rotor and stator walls as

$$\begin{aligned} &\tau_{ri} = -0.03955\rho_i(V_i - R_s\omega\pi/30)^2 \\ &\left(\frac{|V_i - R_s\omega|Dh}{\nu}\right)^{-0.25} \quad \text{sgn}(V_i - R_s\omega\pi/30) \end{aligned}, \tag{6}$$

$$\tau_{si} = 0.03955\rho_i V_i^2 \left(\frac{|V_i|Dh}{\nu}\right)^{-0.25} \quad \text{sgn}(V_i), \tag{7}$$

where Dh is defined as

$$\begin{cases} Dh = \dfrac{2(B+C_r)L_1}{B+C_r+L_1}, & \text{for case1} \\ Dh = \dfrac{2(B+C_r)L_1}{B+C_r+L_1+h}, & \text{for case2, case3} \end{cases}. \tag{8}$$

Further linearization of Eqs. (7) and (8) is accomplished by using perturbation analysis method. The eccentricity of the disturbed rotor is characterized by the perturbation parameter $\varepsilon = e/C_r$, where e is the deviation displacement of the rotor from the cavity center as shown in Fig. 2. Variation of the radial clearance is thus expanded in the following form,

$$\begin{cases} H = C_r + \varepsilon H_1(\theta,t) + \cdots, & \text{for case1, case2} \\ H = (C_r + h) + \varepsilon H_1(\theta,t) + \cdots, & \text{for case3} \end{cases}. \tag{9}$$

Correspondingly, the flow variables are expanded as

$$\begin{aligned} &P_i = P_{0i} + \varepsilon P_{1i}(t,\theta) + \cdots, \\ &V_i = V_{0i} + \varepsilon V_{1i}(t,\theta) + \cdots, \\ &\dot{q}_i = \dot{q}_{0i} + \varepsilon \dot{q}_{1i}(t,\theta) + \cdots, \\ &\tau_{ri} = \tau_{r0i} + \varepsilon \tau_{r1i}(t,\theta) + \cdots, \\ &\tau_{si} = \tau_{s0i} + \varepsilon \tau_{s1i}(t,\theta) + \cdots. \end{aligned} \tag{10}$$

Hence, substituting these linearized variables into Eqs. (3)

and (4) and neglecting the terms of order ε^2 and the higher, the first-order continuity equation for the *i*th cavity is reduced as

$$X_{10}\left(\frac{\partial P_{1i}}{\partial t}+\frac{V_{0i}}{R_s}\frac{\partial P_{1i}}{\partial \theta}+\frac{P_{0i}}{R_s}\frac{\partial V_{1i}}{\partial \theta}\right)+X_{20i}P_{1i-1}+X_{30i}P_{1i} +X_{40i}P_{1i+1}=X_{50i}\left(\frac{\partial H_1}{\partial t}+\frac{V_{0i}}{R_s}\frac{\partial H_1}{\partial \theta}\right), \quad (11)$$

$$Y_{10i}\left(\frac{\partial V_{1i}}{\partial t}+\frac{V_{0i}}{R_s}\frac{\partial V_{1i}}{\partial \theta}\right)+\frac{A_n}{R_s}\frac{\partial P_{1i}}{\partial \theta}+Y_{20i}V_{1i}-q_0V_{1i-1} +Y_{30i}P_{1i-1}+Y_{40i}P_{1i}=Y_{50i}H_1, \quad (12)$$

where $X_{10},X_{20i},X_{30i},X_{40i},X_{50i}$ and $Y_{10i},Y_{20i},Y_{30i},Y_{40i},Y_{50i}$ are functions of the steady pressure and velocity in the *i*th cavity. Subsequently, periodical elliptical orbit (Fig.2) of the rotor center is assumed [15] to solve the linearized first-order continuity Eq. (11) and circumferential momentum Eq. (12). Accordingly, the set of four equations is rearranged in the matrix form,

$$\left[C_i^{-1}\right]\left\{\hat{Y}_{i-1}\right\}+\left[C_i^{0}\right]\left\{\hat{Y}_{i}\right\}+\left[C_i^{+1}\right]\left\{\hat{Y}_{i+1}\right\}=\left\{\hat{A}_i\right\}, \quad (13)$$

where

$$\left\{\hat{Y}_i\right\}=2\left[P_i^{+}/(a-b),P_i^{-}/(a+b),V_i^{+}/(a-b),V_i^{-}/(a+b)\right]^T,$$

$$\left\{\hat{A}_i\right\}=\left[-jG_{5i}\left(\frac{V_{0i}}{R_s}+\Omega\right),-jG_{5i}\left(\frac{V_{0i}}{R_s}-\Omega\right),-X_{5i},-X_{5i}\right]^T.$$

In Eq. (13), $\left[C_i^{-1}\right],\left[C_i^{0}\right]$ and $\left[C_i^{+1}\right]$ are the four-order matrixes of coefficients [15], while P_i^{+},P_i^{-},V_i^{+} and V_i^{-} are constant complex coefficients.

Close inspection of Eq. (13) shows that the four linearized equations are associated with each cavity. For a labyrinth seal with N cavities, this results in a $4(N-1)\times 4(N-1)$ banded system of linear equations set [15], determining the $4(N-1)$ unknowns P_i^{+},P_i^{-},V_i^{+} and V_i^{-} $(i=1,2,\cdots,N-1)$ to obtain the unsteady pressure and shear stress. Subsequently, integrating the unsteady pressure and shear stress in the circumferential direction determines the aerodynamic forcing on the rotor in *x* and *y* directions,

$$F=F_x+jF_y=-\varepsilon\pi R_sL\sum_{i=1}^{N-1}\int_0^{2\pi}\left(P_{1i}e^{j\theta}-ja_r\tau_{r1i}e^{j\theta}\right)d\theta. \quad (14)$$

Based on the force-motion model defined as,

$$-\begin{bmatrix}F_x\\F_y\end{bmatrix}=\begin{bmatrix}K_{xx}&K_{xy}\\-K_{xy}&K_{yy}\end{bmatrix}\begin{bmatrix}x\\y\end{bmatrix}+\begin{bmatrix}C_{xx}&C_{xy}\\-C_{xy}&C_{yy}\end{bmatrix}\begin{bmatrix}x'\\y'\end{bmatrix}, \quad (15)$$

the rotordynamic coefficients characterizing the influence of the aerodynamic forcing exerted by leakage flow through the labyrinth seal with rub grooves are calculated as,

$$K_{xx}=K_{yy}=\frac{1}{2}\mathrm{Re}\left\{J^{+}+J^{-}\right\},$$

$$K_{xy}=K_{yx}=-\frac{1}{2}\mathrm{Im}\left\{J^{+}+J^{-}\right\},$$

$$C_{xz}=C_{yy}=\frac{1}{2\Omega}\mathrm{Im}\left\{J^{+}-J^{-}\right\},$$

$$C_{xy}=C_{yx}=\frac{1}{2\Omega}\mathrm{Re}\left\{J^{+}-J^{-}\right\}, \quad (16)$$

where

$$\begin{cases}J^{+}=\pi R_sL\sum_{i=1}^{N-1}\left[\bar{\hat{Y}}_{2i}\left(1-ja_r\frac{\tau_{r0i}}{P_{0i}}\right)-ja_r\left(\frac{1.75\tau_{r0i}}{V_{0i}-\omega R_s}\bar{\hat{Y}}_{4i}+\frac{0.125\tau_{r0i}D_{h0}}{(B+C_r)^2}\right)\right]\\ J^{-}=\pi R_sL\sum_{i=1}^{N-1}\left[\bar{\hat{Y}}_{1i}\left(1-ja_r\frac{\tau_{r0i}}{P_{0i}}\right)-ja_r\left(\frac{1.75\tau_{r0i}}{V_{0i}-\omega R_s}\bar{\hat{Y}}_{3i}+\frac{0.125\tau_{r0i}D_{h0}}{(B+C_r)^2}\right)\right]\end{cases},$$

for case1, case2

$$\begin{cases}J^{+}=\pi R_sL\sum_{i=1}^{N-1}\left[\bar{\hat{Y}}_{2i}\left(1-ja_r\frac{\tau_{r0i}}{P_{0i}}\right)-ja_r\left(\frac{1.75\tau_{r0i}}{V_{0i}-\omega R_s}\bar{\hat{Y}}_{4i}+\frac{0.125\tau_{r0i}D_{h0}}{(B+C_r+h)^2}\right)\right]\\ J^{-}=\pi R_sL\sum_{i=1}^{N-1}\left[\bar{\hat{Y}}_{1i}\left(1-ja_r\frac{\tau_{r0i}}{P_{0i}}\right)-ja_r\left(\frac{1.75\tau_{r0i}}{V_{0i}-\omega R_s}\bar{\hat{Y}}_{3i}+\frac{0.125\tau_{r0i}D_{h0}}{(B+C_r+h)^2}\right)\right]\end{cases},$$

for case3

2.3 Stability of the rotor

The stabilization and response of the rotor system subject to the aerodynamic forcing is obtained by taking the rotordynamic coefficients into the FEA dynamics equation,

$$[M]\left\{\ddot{Z}\right\}+[C]\left\{\dot{Z}\right\}+[K]\{Z\}=\left\{R\left(\ddot{Z},\dot{Z},\theta,t\right)\right\}. \quad (17)$$

The eigenvalues of Eq. (17) are formulated as $\omega_{ci}+i\delta_i$, where ω_{ci} and δ_i are the ith order critical speed and the ith order logarithmic decrement of the rotor vibration, respectively.

3. Results and discussion

To gain comprehensive understanding of influence of rub grooves on dynamics of the rotor subjected to aerodynamic forcing of the leakage flow, a comparative study was made of flow pattern, leakage rate, rotordynamic coefficients and the logarithmic decrement. Three configurations of the straight-through seal (Fig. 1) with 44 seal teeth on the rotor were chosen for investigation by varying the pressure ratio from 2 to 7 at the constant rotation speed $\omega=3000$ rpm and varying the rotation speed from 1000 rpm to 6000 rpm at the constant pressure ratio 7.

Configuration of the rectangular rub-grooves in [8] was employed here for comparison; the ratio between the rub-groove depth (h) and the clearance (C_r) is 0.6, and the rub-groove width (L_2) is 5 times of the clearance (C_r). As shown in Fig. 1, the axial positions of tooth were chosen as the center and left of the rectangular rub-groove for comparison.

Detailed information of the seal configuration and the working condition was shown in Table 1 and 2, respectively.

A close-up view of the flow pattern (Fig. 3) near the tooth tip was made of influence of rub grooves on the leakage flow at n=7 and $\omega = 3000rpm$. Numerical simulation of the axisymmetric air flow through the labyrinth seals was performed by solving the Navier-Stokes equations and $k-\varepsilon$ turbulence model. The coupling between pressure and velocity was decoupled by using the SIMPLE algorithm [18, 19]. The total computational cells of one seal were 1.4×10^4, 1.5×10^4 and 1.5×10^4 for case 1, case 2 and case 3, respectively. The maximum cell-based residual 10^{-5} was used as the convergence criteria. Sensitivity of the simulation results to the grid density was checked by repeating calculations with different number of cells. The grids in the present work were found to yield satisfactory results. In case 1, the high-speed jet flow at the clearance is restricted by the tooth and the stator wall. As shown in Fig. 3(a), the deflection of the jet flow through the clearance results in vena contraction and decreases the effective flow area due to the separation bubble on the top of the tooth. Accordingly, a part of the pressure head is transformed into local kinetic energy, which is dissipated into heat in the downstream cavity. In case 2, the jet flow through the clearance is slightly deflected into the rub groove, inducing a large recirculation zone near the leading edge of the groove and correspondingly reducing the extent of the vena contract. When the seal tooth is located at the middle station of the groove (Fig. 3(c)), the flow is deflected into the rub groove at high speed, giving rise to a considerable increase of the leakage flow. The influence of rub grooves on the leakage rate at various pressure ratios is shown in Fig. 4. For all cases, the leakage rate is almost linearly increased with increasing the pressure ratio from 2 to 7. In comparison to case 1, slight intensification of the leakage flow in case 2 is observed; the leakage flow increases 0.002 kg/s at n=7. However, a considerable increase of the leakage flow in case 3 is prominent as shown in Fig. 4; deviation of the leakage flow from that in case 1 is enhanced with increasing the pressure ratio, reaching the maximum increase of the leakage flow 0.02 kg/s at n=7.

Prior to investigating the influence of rub grooves on dynamics of the rotor, the single-control-volume method was verified by comparing the calculating results with the experimental results [20]. The straight-through seal (Fig. 1(a)) was chosen and the comparison was made of four different inlet pressure conditions. Comparison of the cross-coupled stiffness coefficients between the calculations and the experiment measurements at various inlet pressures and rotating speeds were shown in Fig. 5. As shown in Fig. 5, with increasing inlet pressure, the cross-coupled stiffness coefficient increases at various rotating speeds. The calculated results are in good consistency to the experimental measurement.

In a view to see influence of rub grooves on dynamics of the rotor subjected to aerodynamic forcing associated with the leakage flow, we calculated the rotordynamic coefficients at

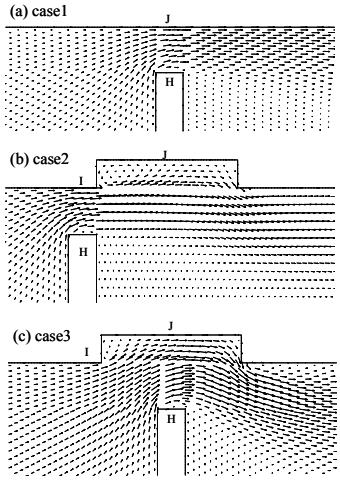

Fig. 3. Close-up view of flow pattern near the seal tooth: (a) case 1, (b) case 2, (c) case 3.

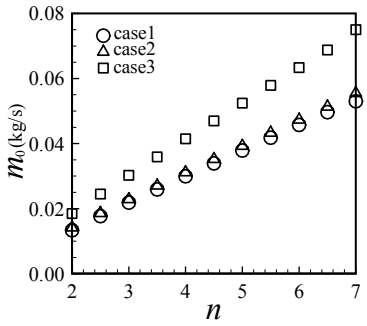

Fig. 4. Variation of leakage flow in respect to the pressure ratio.

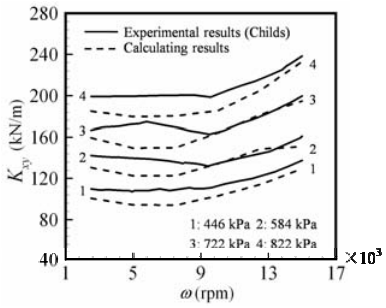

Fig. 5. Comparison of experimental and numerical results of cross-stiffness coefficients.

different pressure ratios (n=2~7) while the rotation speed of the rotor is kept at $\omega = 3000$ rpm and the inlet pre-swirl velocity is set to V_{in}=0 m/s. The variation of the direct stiffness and cross-coupled coefficients in respect to the pressure ratio is shown in Fig. 6. For all cases, the direct stiffness coefficient K_{xx} is linearly proportional to the pressure ratio. On going from n=2 to 7, the deviation of K_{xx} between case1 and case2 is considerably increased from 1.1 kN/m to 3.2 kN/m, while that between case 3 and case 1 is slightly increased from 0.6 kN/m to 0.8 kN/m. These discrepancies of the direct stiffness coefficient indicate the prominent difference in the first critical speed, which is usually estimated as $\sqrt{K_r / M_s}$; here, the

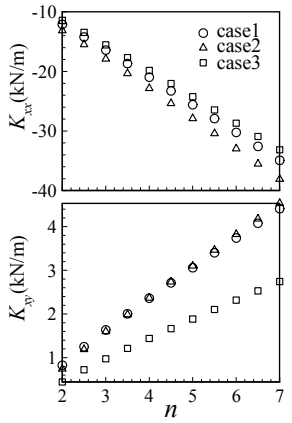

Fig. 6. Variation of stiffness coefficients with increasing the pressure ratio at $\omega = 3000$ rpm: (a) case 1, (b) case 2, (c) case 3.

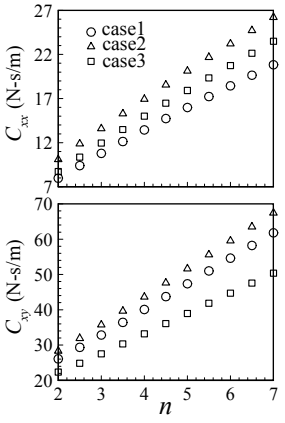

Fig. 7. Variation of damping coefficients with increasing the pressure ratio at $\omega = 3000$ rpm.

parameters K_r and M_s are the modal stiffness and mass of the rotor system, respectively. In computation, the direct stiffness and damping coefficient of the journal bearings are positive. Of noted is that the direct stiffness K_{xx} induced by the leakage flow corresponds to the primary contribution of the aerodynamic forcing to the modal stiffness of the rotor system. In case 2, the prominent decrease of K_{xx} with increasing the pressure ratio gives rise to deformation of the flexible rotor, which is closely related to downshift variation of the first critical speed. In addition, as shown in Fig. 6(b) the cross-coupled stiffness coefficients of all cases gradually increases with increasing the pressure ratio. The difference of the cross-coupled coefficients K_{xy} between case 1 and case 3 significantly increases from 0.38 kN/m at n=2 to 1.7 kN/m at n=7, while that between case1 and case2 is not obviously discerned.

To further understand influence of rub grooves on stability of the rotor-seal system, the direct damping coefficient C_{xx} and cross-coupled damping coefficient C_{xy} were calculated and displayed in Fig. 7. It is obvious in Fig.7 that the coefficients C_{xx} and C_{xy} are also linearly proportional to the pressure ratio for all cases. With increasing the pressure ratio, the difference of C_{xx} between case 1 and case 2 is gradually increased from 2.1 N-s/m at n=2 to 6 N-s/m at n=7, while which between case 1 and case 3 is low to be 0.8 N-s/m at n=2 and 2.6 N-s/m at n=7. Inspecting the coefficients C_{xx} and C_{xy} at different pressure ratios discloses the state $C_{xx}|_{\text{case1}} < C_{xx}|_{\text{case3}} < C_{xx}|_{\text{case2}}$ and $C_{xy}|_{\text{case3}} < C_{xy}|_{\text{case1}} < C_{xy}|_{\text{case2}}$. With increasing the pressure ratio, the difference of C_{xy} between case 1 and case 3 is significantly increased from 3.7 N-s/m at n=2 to 12 N-s/m at n=7, while which between case 1 and case 2 is increased from 2.3 N-s/m at n=2 and 5.7 N-s/m at n=7. The above-mentioned variation of the rotordynamic coefficients reflects the remarkable influence of the rub grooves on dynamics of the rotor.

Prior to conducting further analysis of the stability of the rotor–seal system, we numerically determined distributions of the mean pressure and the circumferential velocity in all cavities for three cases at the condition n=7 and V_{in} = 0 m/s. Inspection of Fig. 8 shows that the mean pressure linearly decreases from the first cavity to the 30th cavity for all three cases, and the descending amplitude of the mean pressure is intensified after the 30th cavity. The presence of rub grooves and the different location of the seal tooth in respect to the rub groove has a slight influence on the mean pressure in cavities. However, distribution of the circumferential velocity in cavities is significant different for all cases. As shown in Fig.8, the circumferential velocity is parabolically increased for all cases. In addition, the slight difference of the circumferential velocity between case 1 and case 2 is found for each cavity, while which between case 1 and case 3 is significantly large. The difference of the circumferential velocity between case 1 and case 3 gradually increases along the axial direction and achieves the largest magnitude 0.8 m/s. The presence of the circumferential velocity in cavity would induce the non-uniform pressure distribution in the circumferential direction of the cavity, which essentially produces the aerodynamic forcing on the rotating rotor. Accordingly, the above-mentioned discrepancy of the circumferential velocity among three cases gives rise to the different rotordynamic coefficients shown in Fig. 6 and Fig. 7. In addition, substituting the mass flow rate and the pressure in each cavity at n=7 into Eq. (1), C_0 was determined to 0.77, 0.64 and 0.78 for case1, case2

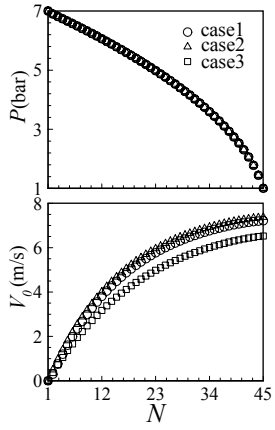

Fig. 8. Distributions of the mean pressure and circumferential velocity in cavities at n=7 and V_{in} =0 m/s: (a) case 1, (b) case 2, (c) case 3.

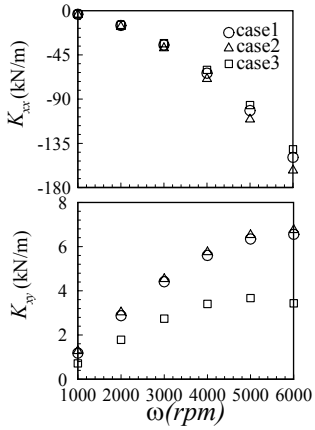

Fig. 9. Variation of stiffness coefficients with increasing the rotating speed at n=7 and V_{in}=0 m/s: (a) case 1, (b) case 2, (c) case 3.

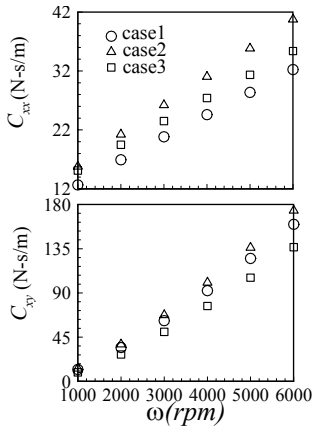

Fig. 10. Variation of damping coefficients with increasing the rotating speed at n=7 and V_{in}=0 m/s: (a) case 1, (b) case 2, (c) case 3.

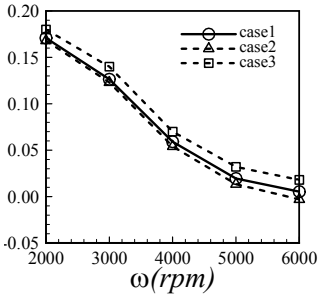

Fig. 11. Variation of logarithmic decrement with increasing the rotating speed for three cases.

and case3, respectively.

Now we turn to see influence of rub grooves on stability of the rotating rotor system. Recall that the rotating speed of the rotor has very slight influence on the leakage mass flow rate [6], the stabilization analysis of the rotating rotor with the increase of the rotating speed ω from 1000 rpm to 6000 rpm at n=7 and V_{in}=0 m/s was performed. Influence of rub grooves on the rotordynamic coefficients is shown in Fig. 9 and Fig. 10. As shown in Fig. 9, the parameter K_{xx} decreases with increasing ω for all cases. The difference of K_{xx} between case 1 and case 2 is gradually increased with increasing ω, achieving the maximum deviation 13.3kN/m at $\omega = 6000$ rpm. Similar variation of the gap between K_{xx} of case 1 and case 3 is shown in Fig. 9, reaching 8.2 kN/m at $\omega = 6000$ rpm. In addition, the parameter K_{xy} of all three cases and the gap between K_{xy} of different cases are increased with increasing ω; the magnitude gap $\left|K_{xy\_case1} - K_{xy\_case3}\right|$ is significantly increased with increasing ω, reaching the peaked magnitude 3.1 kN/m at $\omega = 6000$ rpm. As shown in Fig. 10, the parameters C_{xx} and C_{xy} linearly increase in respect to ω. Furthermore, the magnitude gaps $\left|C_{xx\_case1} - C_{xx\_case2}\right|$ and $\left|C_{xx\_case1} - C_{xx\_case3}\right|$ are peaked to 9 N-s/m and 3 N-s/m at $\omega = 6000 rpm$, respectively. Subsequently, numerical prediction of the destabilization of the rotor, which is resulted from the leakage through the seals of three cases, was given in terms of the logarithmic decrement δ_1 of the rotor vibration. Destabilization of the rotor emerges when δ_1 is less than 0. As displayed in Fig. 11, the logarithmic decrements of all three cases at n=7 are decreased with increasing the rotating speed. For case 1 and case 3, the rotor system is kept at the stable operation, while the destabilization of the rotor is found at $\omega = 5800$ rpm for case2. In addition, according to the definition of the whirl frequency ratio ($\Omega_f = K_{xy} / \left(C_{xx} \cdot \Omega\right)$) where Ω is rotor whirling speed, the stability of the rotor decreased with increasing ω. Furthermore, $\Omega_f\big|_{case2} = 0.95 > \Omega_f\big|_{case1} = 0.83 > \Omega_f\big|_{case3} = 0.61$ was obtained at $\omega = 6000$ rpm. This demonstrates that the aerodynamic forcing in case 2 intensifies the destabilization of the rotor system.

4. Conclusions

Influence of rub grooves on dynamics and stability of the rotor subjected to aerodynamic forcing associated with leakage flow through 44 straight-through seals was quantitatively and qualitatively studied by using numerical calculations based on the single control-volume method and the perturbation analysis. Three cases, e.g. the seal without rub grooves (case1), the seal with upstream shifting of the seal tooth in respect to the rub groove (case2) and the seal with location of the seal tooth in the middle station of the rub groove (case3), were chosen for the comparative study. The discharge coefficient at the orifice for three cases was numerically determined by using CFD. Influence of rub grooves on the leakage flow was analyzed in terms of the close-up view of the flow pattern near the seal tooth, leakage flow rate, distributions of the mean pressure and circumferential velocity in cavities. In comparison to case 1, the presence of the rub groove in case 3 significantly increases the leakage flow rate, while a weak increase is found in case 2. Numerical results of the rotordynamic coefficients for all systems disclosed the considerable influence of rub grooves on dynamics of the rotor. The significant discrepancy of rotordynamic coefficients in cases with rub grooves from the normal case (case 1) was revealed by varying the pressure ratio and the rotating speed. In addition, influence of rub grooves on stability of the rotor system was evaluated by

determining the logarithmic decrement; the results demonstrated that the aerodynamic forcing in case 2 intensifies the destabilization of the rotor system.

Acknowledgment

This work was supported by Key Project of Chinese Ministry of Education (No.309012) and national Natural Science Foundation of China (No. 50906049 and 10732060), China.

Nomenclature

A	:	Unsteady cross-sectional area of the cavity [m^2]
A_n	:	Steady annular flow area [m^2]
B	:	Tooth height [m]
$[C]$	:	Damping matrix
C_0	:	Orifice contraction coefficient
C_1	:	Kinetic energy carry-over coefficient
C_r	:	Steady radial seal clearance [m]
C_{xx}, C_{yy}	:	Damping coefficients [N-s/m]
C_{xy}, C_{yx}	:	Cross-couple damping coefficients [N-s/m]
D_{h0}	:	Steady hydraulic diameter of the cross-sectional area of the cavity [m]
F	:	Total air reaction force [N]
F_x, F_y	:	Annular seal reaction force components [N]
H	:	Unsteady height of the cavity [m]
h	:	Height of rub groove [m]
$H_1(\theta,t)$	:	Perturbation radial clearance [m]
j	:	Imaginary number
K_{xx}, K_{yy}	:	Direct stiffness coefficients [N/m]
K_{xy}, K_{yx}	:	Cross-couple stiffness coefficients [N/m]
$[K]$	:	Stiffness matrix
L_1	:	Cavity length [m]
L_2	:	Length of rub groove [m]
m	:	Mass flow rate [kg/s]
$[M]$	:	Mass matrix
N	:	Tooth number
P_{0i}, P_i	:	Steady and unsteady pressures in the ith cavity [Pa]
$P_{1i}(\theta,t)$	:	Perturbation pressure in the ith cavity [Pa]
$\dot{q}_{0i}, \dot{q}_i$	:	Steady and unsteady leakage flow rate per unit length in the ith tooth [kg/s-m]
$\dot{q}_{1i}(t,\theta)$	:	Perturbation leakage flow rate per unit length [kg/s-m]
R	:	Gas constant [J/kg-K]
R_s	:	Rotor radius [m]
$\{R(\ddot{Z},\dot{Z},\theta,t)\}$	:	Load tensor
T	:	Gas temperature in the labyrinth seal [K]
U	:	Sliding speed of the rotor surface [*rpm*]
V_{0i}, V_i	:	Steady and unsteady circumferential velocities in the ith cavity [m/s]
$V_{1i}(t,\theta)$	:	Perturbation pressure at the ith cavity [m/s]
V_{in}	:	Inlet pre-swirl velocity [m/s]
(x,y)	:	x and y coordinates of rotor whirling motion
X	:	Coordinate along the circumference of the cavity
Y	:	Coordinate across the length of the cavity
$\{Z\}$	:	Displacement tensor
$\{\dot{Z}\}$	:	Velocity tensor
$\{\ddot{Z}\}$	:	Acceleration tensor

Greek symbols

μ	:	Dynamic viscosity of fluid [kg/m-s]
τ_{r0i}, τ_{ri}	:	Steady and Unsteady shear stress at the rotor wall [N/m^2]
$\tau_{r1i}(\theta,t)$	:	Perturbation shear stresses at the rotor wall [N/m^2]
τ_{s0i}, τ_{si}	:	Steady and unsteady shear stresses at the stator wall [N/m^2]
$\tau_{s1i}(t,\theta)$	:	Perturbation shear stresses at the stator wall [N/m^2]
ε	:	Eccentricity ratio
ρ_i	:	Gas density of the ith cavity [kg/m^3]
θ	:	Azimuthal position
α_r	:	Dimensionless shear stress length at the rotor wall
α_s	:	Dimensionless shear stress length at the stator wall
ω	:	Rotor rotating speed [*rpm*]
ω_d	:	Destabilization rotating speed [*rpm*]
ω_{ci}	:	The ith order critical speed [*rpm*]
Ω	:	Rotor whirling speed [*rpm*]

References

[1] D. L. Rhode and R. G. Adams, Rub-groove width and depth effects on flow predictions for straight-through labyrinth seals, *ASME Journal of Tribology*, 126 (2004) 781-787.

[2] A. Picardo and D. W. Childs, Rotordynamic coefficients for a tooth-on-stator labyrinth seal at 70 bar supply pressures: measurements versus theory and comparison to a hole-pattern stator seal, *ASME Journal of Engineering for Gas Turbines and Power*, 127 (2005) 843-855.

[3] K. Kwanka, Dynamic coefficients of stepped labyrinth gas seals, *ASME Journal of Engineering for Gas Turbines and Power*, 122 (2000) 473-477.

[4] Y. Z. Liu, W. Z. Wang and H. P. Chen, *et.al.* Influence of leakage flow through labyrinth seals on rotordynamics: numerical calculations and experimental measurements, *Arch. Appl. Mech.*, 77 (2007) 599-612.

[5] H. Zimmerman, A. Kammerer and K. H. Woff, Performance of worn labyrinth seals, *ASME 94-GT-131*, 1994.

[6] Z. Yu and D.W. Childs, Experimental rotordynamic coefficient and static characteristic results for a labyrinth rotor running against a grooved stator with L/D=0.466, C_r/r=0.0036, *Mechanical Engineering Department, Turbomachinery Laboratories, Texas A&M University*, 1995.

[7] D. L. Rhode and R. G. Adams, Computed effects of rub-grooves size on stepped labyrinth seal performance, *STLE*

Tribology Transactions, 44 (2001) 523-532.

[8] J. M. Xu, M. S. Ambrosia and D. L. Rhode, Effect of rub-groove shape on the leakage of abradable stepped labyrinth seals, *AIAA-2004-3718*, 2004.

[9] J. Denecke, V. Schramm, S. Kim and S. Witting, Influence of rub-grooves on labyrinth seal leakage, *ASME Journal of Turbomachinery*, 125 (2003) 387-393.

[10] D. L. Rhode and R. G. Adams, Relative axial displacement leakage effects on straight-through labyrinth seals with rub grooves, *AIAA-2004-3716*, 2004.

[11] P. A. E. Steward and K. A. Brasnett, The contribution of X-ray to gas turbine air sealing technology, *AGARD Conf. Proc.*, 237 (1978) 1-13.

[12] D. W. Childs, L. E. Rodriguez and V. Cullotta, *et.al*., Rotordynamic-coefficients and static (equilibrium loci and leakage) characteristics for short, laminar-flow annular seals, *Transactions of the ASME, Journal of Tribology*, 128 (2006) 378-387.

[13] M. S. Graviss, The influence of a central groove on static and dynamic characteristics of annular liquid seal with laminar flow, *Texas A&M University, USA*, 2005.

[14] G. G. Hirs, Fundamentals of a bulk-flow theory for turbulent lubrication films, *Ph.D. Dissertation, Delft Technical University, The netherlands* 1970.

[15] E. Dursun and J. Y. Kazakia, Air flow in cavities of labyrinth seals, *Int. J.Eng. Sci.*, 33 (1995) 2309-2326.

[16] D.W. Childs and J. K. Scharrer, An Iwastsubo-based solution for labyrinth seals: comparison to experimental results, *ASME J. Eng. Gas Turbines Power*, 108 (1986) 325-331.

[17] J. Denecke, V. Schramm, S. Kim and S. Witting, Influence of rub-groove on labyrinth seal leakage, ASME Journal of Turbomachinery, 125 (2003) 387-393.

[18] W. Z. Wang and Y. Z. Liu, Numerical analysis of leakage flow through tow labyrinth seals, *Journal of Hydrodynamics Ser. B*, 19 (2007) 107-112.

[19] J. P. Van Doormall and G. D. Raithby, Enhancement of the SIMPLE method for prediction incompressible fluid flows, *Numerical Heat Transfer*, 7 (1984) 147-163.

[20] D. W.Childs and J. K. Scharrer, Theory versus experiment for the rotordynamic coefficients of labyrinth gas seals: Part II – A comparison to experiment, *Journal of Vibration, Acoustics, Stress, and Reliability in Design*, 110 (1988) 281-287.

Wei Zhe WANG is currently a research assistant at School of Mechanical Engineering, Shanghai Jiao Tong University, China. His research interests are flow-induced vibration in turbomachinery, advanced sealing technology, advanced computational fluid dynanmics, and nonlinear flow-structure analysis.

Ying Zheng LIU is currently a professor at School of Mechanical Engineering, Shanghai Jiao Tong University, China. His research interests are flow control, separated flow, and flow and structure analysis of thermal system.